LA-UR-01-4909
Approved for public release; distribution is unlimited.

Title: **DYNAMIC MELT RATE CONTROL ON A LABORATORY SCALE VAR FURNACE WITHOUT LOAD CELL FEEDBACK**

Author(s): Rodney L. Williamson, Joseph. J. Beaman, David K. Melgaard, Gregory J. Shelmidine, Phillip K. Tubesing, and Robert M. Aikin, Jr.

Submitted to:

http://lib-www.lanl.gov/cgi-bin/getfile?00796837.pdf

DYNAMIC MELT RATE CONTROL ON A LABORATORY SCALE VAR FURNACE WITHOUT LOAD CELL FEEDBACK

Rodney L. Williamson[a], Joseph. J. Beaman[b], David K. Melgaard[a], Gregory J. Shelmidine[a], Phillip K. Tubesing[c], and Robert M. Aikin, Jr.[c]

[a] Liquid Metals Processing Laboratory
Sandia National Laboratories
Albuquerque, New Mexico 87185-1134

[b] Department of Mechanical Engineering
University of Texas
Austin, Texas 78723

[c] Materials Science and Technology Division
Los Alamos National Laboratory
Los Alamos, New Mexico 87545

ABSTRACT

Based on a linearized version of an accurate, low order, dynamic melt rate model, a feedback melt rate controller was designed and tested on a small VAR furnace at Los Alamos National Laboratory. Model based control was necessary because the furnace is not equipped with a working load cell transducer. The model was incorporated into a process filter that produces estimates of electrode thermal boundary layer, electrode gap, electrode position and electrode mass. Estimated values for the thermal boundary layer and electrode gap were used for feedback. The input commands were melting current and electrode drive speed. A test melt was performed wherein a 0.127 m diameter 304SS electrode was melted into 0.165 m diameter ingot at a nominal melt rate of 27 g/s. Toward the end of the test, a melt rate step up to 32 g/s was commanded. The controller initiated a nonlinear current ramp to produce the commanded step. Electrode position data were analyzed and the results used to determine that the actual melt rate profile followed the commanded profile relatively well.

INTRODUCTION

Over the past several years, Sandia National Laboratories (SNL), Los Alamos National Laboratory (LANL), and the Specialty Metals Processing Consortium (SMPC) have invested significant resources into improving control of the vacuum arc remelting (VAR) process. The goal of this work has been, and continues to be, producing specialty metal alloy products with better properties. One of the focus areas of this work has been developing better melt rate control because it is felt that the current generation of VAR controllers have some serious shortcomings.

First, modern VAR control systems are unable to accurately generate relatively steep melt rate ramps. For example, suppose one wishes to initiate a linear melt rate ramp over a one minute period, as one might do as part of a startup or hot-top procedure. This is very difficult to achieve in practice because the melt rate ramp duration is short relative to the time required to achieve steady state thermal conditions in the electrode. If one attempts to produce the melt rate ramp with a linear current ramp, a highly nonlinear melt rate condition is produced wherein one either over- or undershoots the final melt rate target depending on the direction of the ramp. After the initial transient, the melt rate gradually relaxes to the steady state value corresponding to the current setpoint as the thermal distribution in the electrode relaxes to its new steady state.[1] Depending on the material and size, this can take up to a few hours.

Another difficulty with achieving melt rate control arises because modern VAR control systems require electrode weight data from a load cell transducer for feedback. Because these data are relatively noisy, the data must be averaged or a regression analysis performed so as to obtain reliable melt rate information. This gives rise to melt rate control that is relatively highly damped. Because the controller only "knows" about the average past, it cannot respond to melt rate disturbances that occur on a time scale that is short compared to that over which the load cell data are being processed. For example, it is not uncommon to perform regression analysis on data acquired over a time period of ten or twenty minutes, making for a fairly unresponsive system that cannot be tuned to correctly respond to melt rate disturbances introduced by cracks and welds.

The melting dynamics problem may be overcome by supplying the furnace with a nonlinear current schedule corresponding to the desired linear melt rate ramp. This requires that one obtain the relevant current schedule either through a dynamic electrode melting model or by trial and error. Open loop melt rate control of this type has been reported by Bertram et al. for 0.43 m (17 inch) diameter Alloy 718.[2] They used a melting dynamics code to derive the current schedule required to produce a series of relatively large melt rate steps. When implemented, the schedule produced the predicted steps with little over- or undershoot, demonstrating the feasibility of model based melt rate control.

Of course, the problem with open loop control is that it cannot respond to changing melting conditions or process disturbances. Also, a current schedule must be specifically designed ahead of time for each melt rate ramp required. Therefore, solving the dynamic melt rate problem requires a closed loop controller that tracks the thermal conditions in the electrode and calculates the appropriate current response "on the fly." Such a controller is described by Beaman et al. in a companion paper.[3] The controller employs measurements and a low order, nonlinear melting model to track thermal conditions in the electrode throughout the melt. The method of control presented does not require heavily filtered or regressed load cell data. Indeed, although load cell data are highly desirable for improved performance, the controller does not require load cell data at all. Furthermore, electrode gap is simultaneously and independently controlled using this means of control.[4]

This paper reports the implementation and preliminary testing of the dynamic VAR process controller described in Ref. [3]. Dynamic, in this case, means that the process variables are changed on a time scale that is short compared to the time required for the thermal distribution in the electrode to reach steady state. This technology enables melting engineers to easily implement extremely aggressive melt rate schedules while simultaneously maintaining accurate control of electrode gap, allowing execution of the "optimized" VAR process recipes suggested by the latest generation of predictive simulation tools. Furthermore, it makes this possible on furnaces that are not equipped with load cell transducers to measure electrode mass. The test work described herein was performed on the small VAR furnace at the LANL uranium foundry while melting 304 stainless steel.

CONTROLLER IMPLEMENTATION

The process variables of interest for the controller are as follows: M – electrode mass; $\dot{M}$ – electrode melting rate; G – electrode gap; I – melting current; V_{ram} – ram velocity; X or X_{ram} – ram position; Δ – electrode thermal boundary layer thickness; and μ – melting efficiency. These are discussed fully in Ref. [3].

The state variables for the process are Δ, G, X, μ and M. Because the LANL furnace was not equipped with a functioning load cell transducer at the time this test was performed, there is no measurement value for M. There are also no measurements available for Δ and μ. Thus, the only available measured state variables are G and X. X was measured using a Temposonics transducer (MTS Systems Corp., Eden Prairie, MN) with a precision of ±0.003 m. G was not truly measured, but estimated from drip-short data using a measurement model.[5] The model is given by

$$G(I, f_{DS}) = 965 I^{-0.595} f_{DS}^{-0.669} \qquad (1)$$

where f_{DS} is the drip short frequency in s^{-1}, I is in amperes and G is in centimeters. The error in this model for a 2 s average is ±1.5 cm.

Figure 1 shows a diagram of the linearized dynamic melt rate controller implemented on the LANL VAR furnace. As in Ref. [3], a "0" subscript indicates the nominal value for the associated variable about which the controller was designed, and a "d" in front of the variable denotes the difference between the variable and its nominal value. With reference to the diagram, the nominal values of the controller inputs are subtracted from the reference inputs to generate the reference difference inputs, $d\dot{M}_{ref}$ and dG_{ref}. These are operated on by K_r, the reference input gain matrix, to generate difference current and ram velocity command variables, dI_c and $dV_{ram,c}$, which are then corrected by feedback and feedforward data. The nominal values are then added to form the commanded current and drive speed variables to the furnace. However, because the LANL furnace employs a simple hydraulic cylinder drive system, it is difficult to command a wide range of velocities without generating significant errors, even with careful characterization of the drive system. Therefore, the velocity variable is integrated and the result added to the nominal position to give a commanded electrode position, $X_{ram,c}$. Thus, commanded current and ram position constitute the actual inputs to the VAR process.

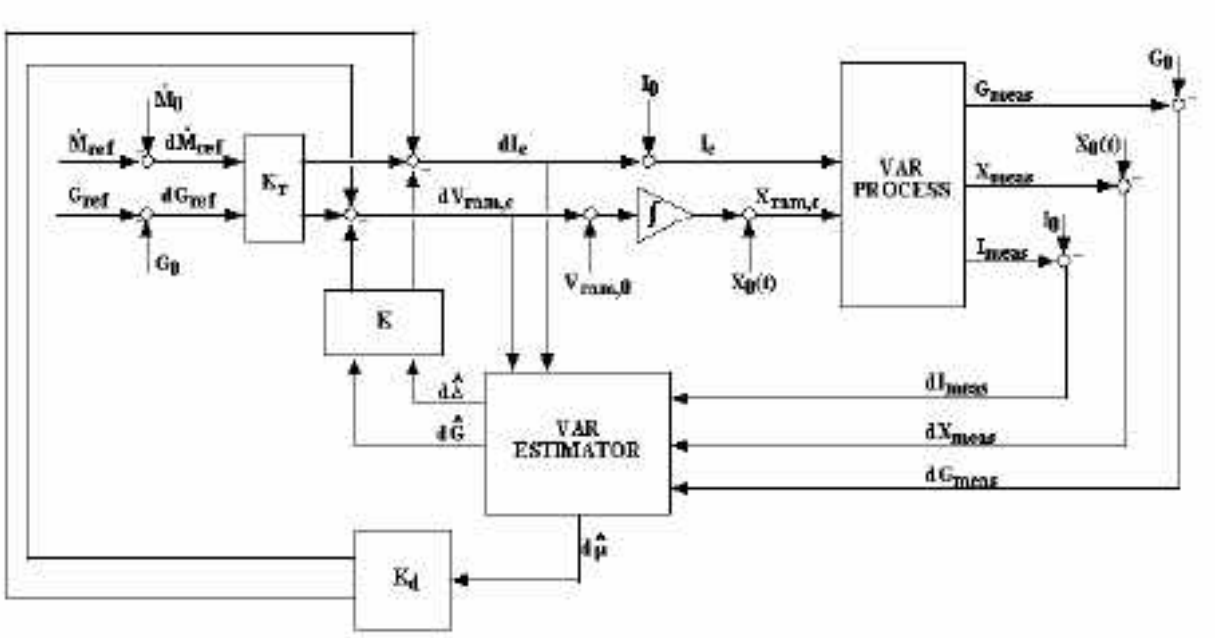

Figure 1. Schematic diagram of the linear dynamic melt rate controller implemented on the VAR furnace at the Los Alamos National Laboratory uranium foundry.

Three furnace outputs are measured and used by the controller: G_{meas}, X_{meas} and I_{meas}. The nominal values associated with these variables are subtracted from the measurements to generate difference measurement variables that are fed into the VAR Estimator (Kalman filter). The estimator also requires dI_c and $dV_{ram,c}$ as inputs. The outputs of the estimator are estimated difference values for thermal boundary layer, electrode gap and efficiency. $d\hat{\Delta}$ and $d\hat{G}$ are operated on by the feedback gain matrix, K, and the results used to correct the difference control inputs. $d\hat{\mu}$ is operated on by the feedforward disturbance gain matrix, K_d, and used to correct the control inputs for efficiency disturbances.

The control law may be summarized by the following simple equation:

$$\mathbf{u}_n = \mathbf{K_r y_r} - \mathbf{K}\hat{\mathbf{x}}_{\mathbf{c}_n} + \mathbf{K_d}\hat{\mathbf{x}}_{\mathbf{d}} \tag{2}$$

where $\mathbf{u}$ is the control input vector, $\mathbf{y_r}$ is the reference output, $\hat{\mathbf{x}}_{\mathbf{c}}$ is the estimated control state, and $\hat{\mathbf{x}}_{\mathbf{d}}$ is the estimated disturbance state.

The function of the VAR Estimator is to produce estimates of the process state variables from the inputs and measured outputs. By definition, the current state of the process is specified once the process state variables are determined. The estimator is described by the following expressions:

$$\hat{\mathbf{x}}(n+1\,|\,n+1) = \hat{\mathbf{x}}(n+1\,|\,n) + \mathbf{M}\left[\mathbf{z}(n+1) - \mathbf{H}\hat{\mathbf{x}}(n+1\,|\,n) - \mathbf{F_u u}(n)\right] \tag{3}$$

$$\hat{\mathbf{x}}(n+1\,|\,n) = \Phi\hat{\mathbf{x}}(n\,|\,n) + \Gamma\mathbf{u}(n) \tag{4}$$

where n refers to the n^{th} time step, a hat-symbol denotes an estimated quantity, **x** denotes the vector composed of the five state variables, **z** is a vector comprised of the three measured variables, and Φ, Γ, **M**, **H**, and $\mathbf{F_u}$ are matrix operators used to describe the dynamics of the system. Eq. 3 reads: The updated estimate of **x** is equal to the estimate of **x** generated by projecting the previous estimate forward in time using the dynamic system model (Eq. 4) corrected by a factor related to the difference between latest measured outputs, **z**(n+1), and the outputs estimated from the dynamic system model, $\mathbf{H}\hat{\mathbf{x}}(n+1|n)$. The form and values of the matrix operators are derived from a state-space model of the process as reported in Ref. [3]. Φ is the state transition matrix and defines how the process evolves from one time step to the next under nominal conditions with no inputs. The input matrix, Γ, defines how the state evolves due to the applied inputs. **H** is the measurement (or output) matrix. It operates on the state estimate to produce the estimated outputs. These are subtracted from the measured values. $\mathbf{F_u}$ is the throughput matrix and defines which of the inputs are directly coupled to which measured variables. The quantity in square brackets in Eq. 3 is often called the innovation. It is an indication of how well the measurements match the model-based estimates. When operated on by the Kalman matrix, **M**, the result forms a correction to the projected state estimate. The elements of **M** are weighting factors that determine the relative weights of the model predictions compared to the measurements. For example, if a particular measurement is known to be very noisy, its contribution will not be weighted heavily and the corresponding element in **M** will be small. M is obtained by solving the algebraic Ricatti equation after characterizing the process model and measurement noise terms (see Ref. [3]).

Figure 2 shows a schematic diagram of the hardware implementation of the controller at LANL. The Pentium™ computer was equipped with two PCI-MIO-16XE cards from National Instruments (Austin, TX) for data I/O. Voltage data were acquired using one of the analog input channels of card #1. These data were analyzed by the computer to obtain drip-short frequency data. Signal conditioning was achieved using Analog Devices (Norwood, MA) isolation amplifiers as depicted in the figure. Current data were acquired from a shunt (5 mV/kA). Ram position was controlled using an Oilgear (Milwaukee, WI) servo valve amplifier. This device is equipped with an internal PI controller designed to drive the error between X_{ref} ($X_{ram,c}$ in Figure 1) and X_{meas} to zero. The hardware was designed so that a single switch actuated the control relay taking current and ram control from the furnace PLC. All other normal PLC functions were left intact.

As mentioned above, implementation of the controller requires knowledge of the noise characteristics of the process and measurements. These are listed in Ref. [3] but are summarized here for convenience. Table 1 lists the nominal values, Table 2 the process noise and measurement noise terms.

TABLE 1

Variable	Nominal Value
μ_0	0.419
I_0	3884 A
Δ_0	6.93 cm
$V_{ram,0}$	0.00971 cm/s

TABLE 2

Noise Term	Strength
σ_I	82 A
$\sigma_{V_{ram}}$	0.00049 cm/s
σ_μ	6.93 $s^{-1/2}$
$\sigma_{I_{meas}}$	75 A
$\sigma_{X_{ram}}$	0.3 cm
$\sigma_{G_{ds}}$	1.5cm

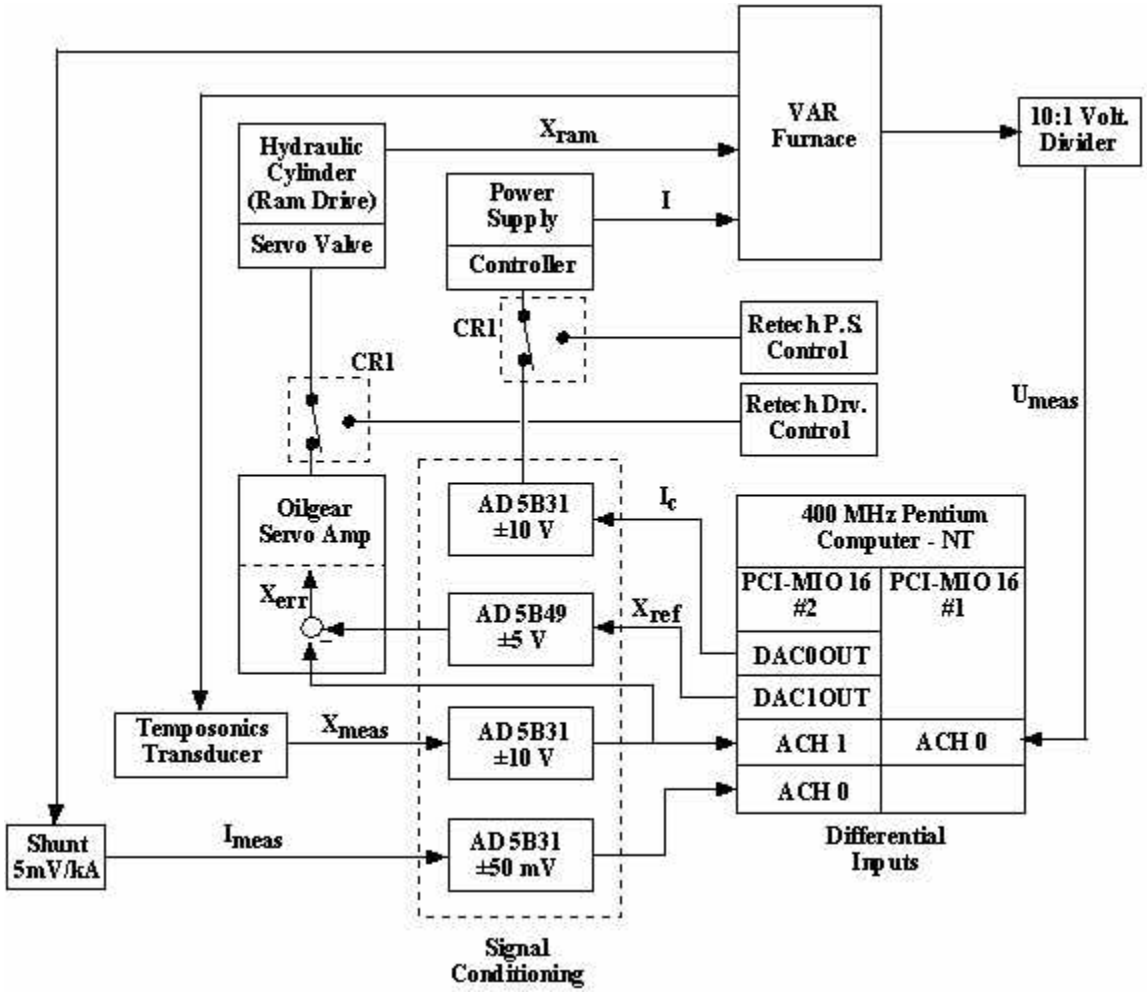

Figure 2. Schematic diagram of the hardware used to implement the dynamic melt rate controller on the VAR furnace at the Los Alamos National Laboratory uranium foundry.

CONTROLLER PERFORMANCE

The test melt involved melting a 0.127 m (5.0 inch) diameter 304 stainless steel electrode into 0.165 m (6.5 inch) diameter ingot at a steady-state melt rate of 27 g/s. Near the end of the melt, an "instantaneous" melt rate step to 32 g/s was implemented. The voltage and current traces associated with this exercise are shown in Figure 3. Note from the figure that the current steps up immediately by 300-400 amperes to accomplish the melt rate step, but approaches the steady state value associated with the new melt rate in a highly nonlinear manner. This is, indeed, the expected behavior; but is the melt rate actually being controlled to the input reference?

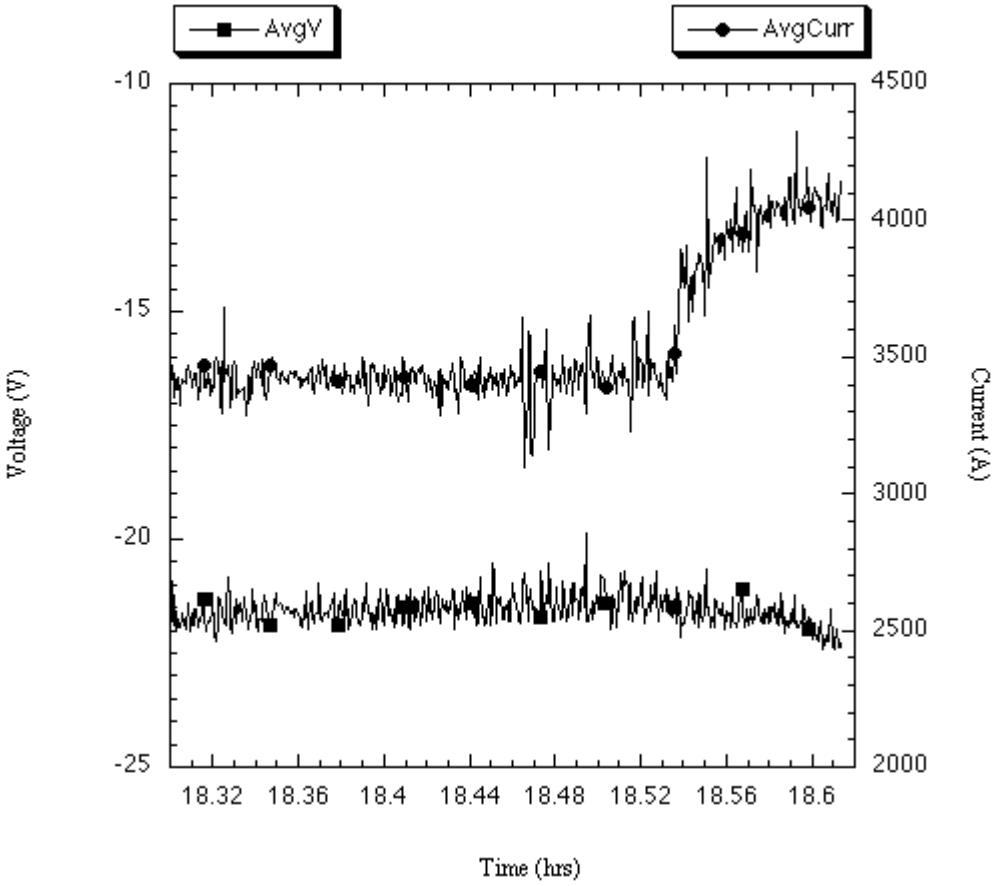

Figure 3. Plot of voltage and current traces showing the region of the melt where the melt rate step was implemented.

Figure 4 shows the melt rate reference trace along with the measured position trace. Because no electrode weight data are available, melt rate must be estimated from the position data. Melt rate can be estimated from the ram velocity using the following equation:

$$\dot{M} = \frac{\rho_L A_e V_{ram}}{1 - \frac{A_e}{A_i}} = \frac{\rho_L A_e V_{ram}}{a} \tag{5}$$

where ρ_L is the liquid density, and A_e and A_i are the electrode and ingot cross sectional areas, respectively, and *a* is the geometric fill ratio factor (Ref. [3], Eq. 25). Regressions were performed to fit the position data in the two melting regions to straight lines and the results are plotted in Figure 4. The slopes of the two lines are 40.5 cm/hr (±0.8 cm/hr, R^2_{fit} =0.97) and 48.8 cm/hr (±2.9 cm/hr, R^2_{fit} =0.88) for the low and high melt rate regions, respectively. The uncertainties represent 95% confidence limits on the slopes. The ratio of these two numbers is 0.83. The ratio of the target melt rates is 0.84, indicating that the controller is performing, on average, as expected. Using 7.0 g/cm^3 for the density of liquid stainless steel at superheat and the above slopes in Eq. 5 gives average melt rate values of 24.5±0.5 g/s and 29.6±1.8 g/s for the two melting regions, both slightly below the targets of 27 g/s and 32 g/s. However, the controller applies an experimental correction to the geometric fill ratio factor to account for thermal effects. The correction is equal to 0.942. When this is used in Eq. 5, the observed average melt rates are 26.0±0.5 g/s and 31.4±1.8 g/s, much closer to the reference values.

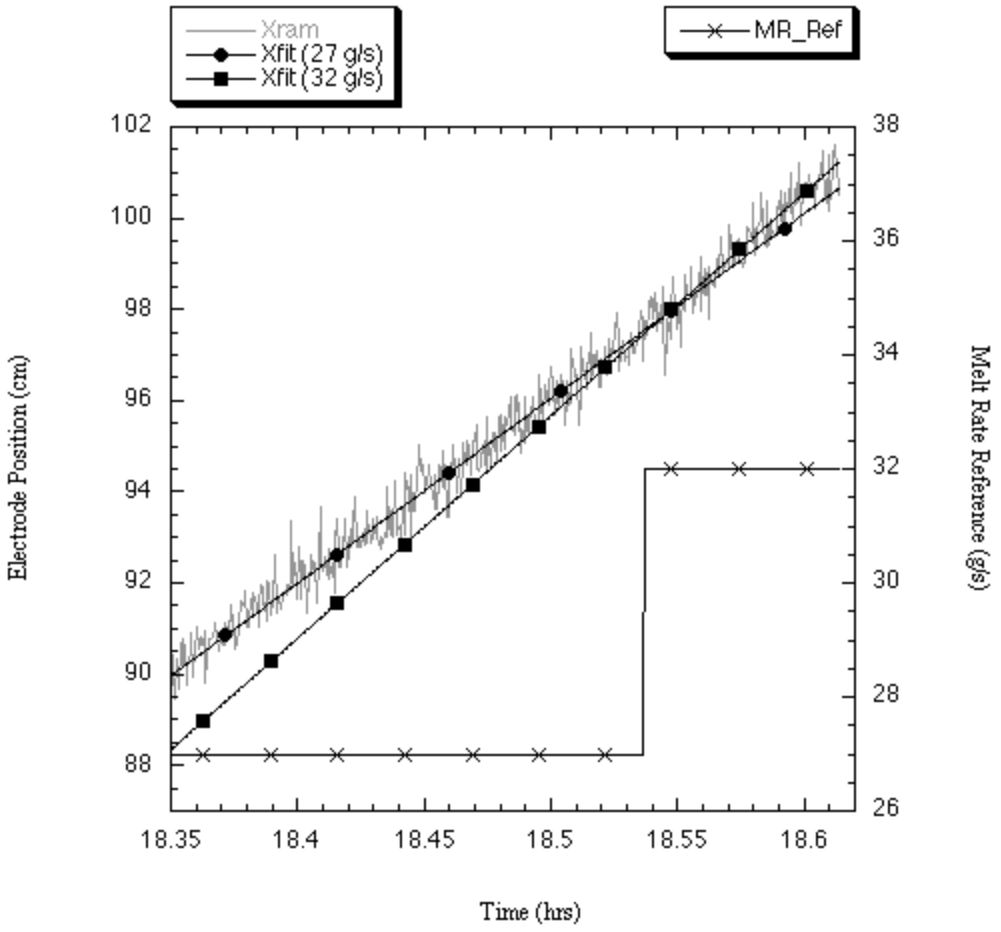

Figure 4. Plot of ram position and melt rate reference traces in the region of the melt where the melt rate step was implemented. The straight lines are the results of linear regressions.

Finally, Figure 5 shows a plot of drip-short frequency over the same melt region as the plot in Figure 4. The large deviation at around 18.35 hours is associated with melting through the point at which the two pieces which comprise the electrode were welded together. Note also that the average "measured" gap drops below the reference value of 1.0 cm to about 0.8 cm

between ~18.42 and ~18.46 hours but that the Kalman filtered value remains constant over this interval. The event at ~18.51 hours during which drip-shorts all but disappeared was associated with a short glow condition. Figure 6 shows drip-short and ram position data in the region of the weld disturbance. It is apparent from the data that the controller controls average melt rate through this region. The calculated value for the region shown is 25.0±0.7 g/s, in agreement with the above value. However, during the ~145 s weld event itself, the calculated melt rate is 29.3±4.4 g/s.

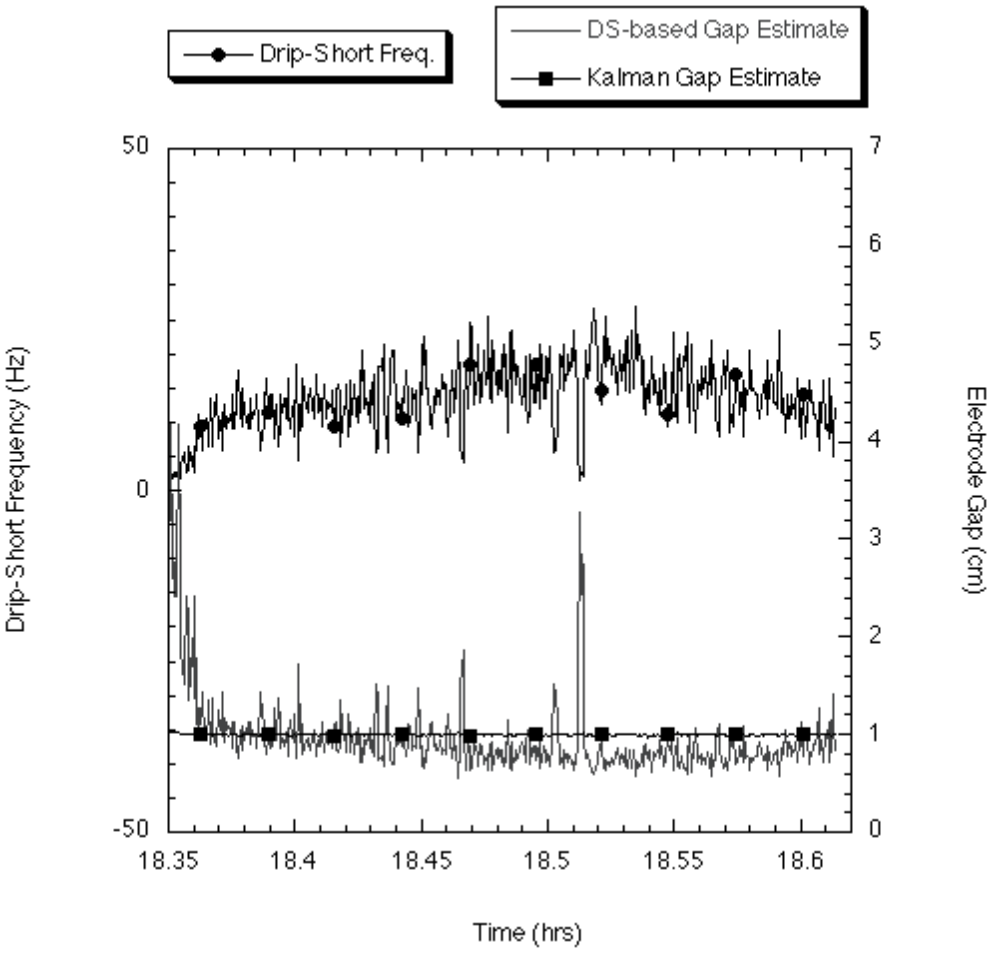

Figure 5. Plot of drip-short frequency, and electrode gap estimated from drip-short frequency and from the Kalman filter.

DISCUSSION

Because of the relatively noisy ram position data, it is impossible to say what the step-to-step variation in melt rate is. For example, when using a 60 s sliding average, the 27 g/s test region yields an average calculated melt rate of 25.5 g/s, relatively close to the target value, but with a standard deviation of 19.8 g/s, nearly 80% as large as the mean. However, the results shown in Figure 4 provide strong evidence for average melt rate control over the time intervals investigated.

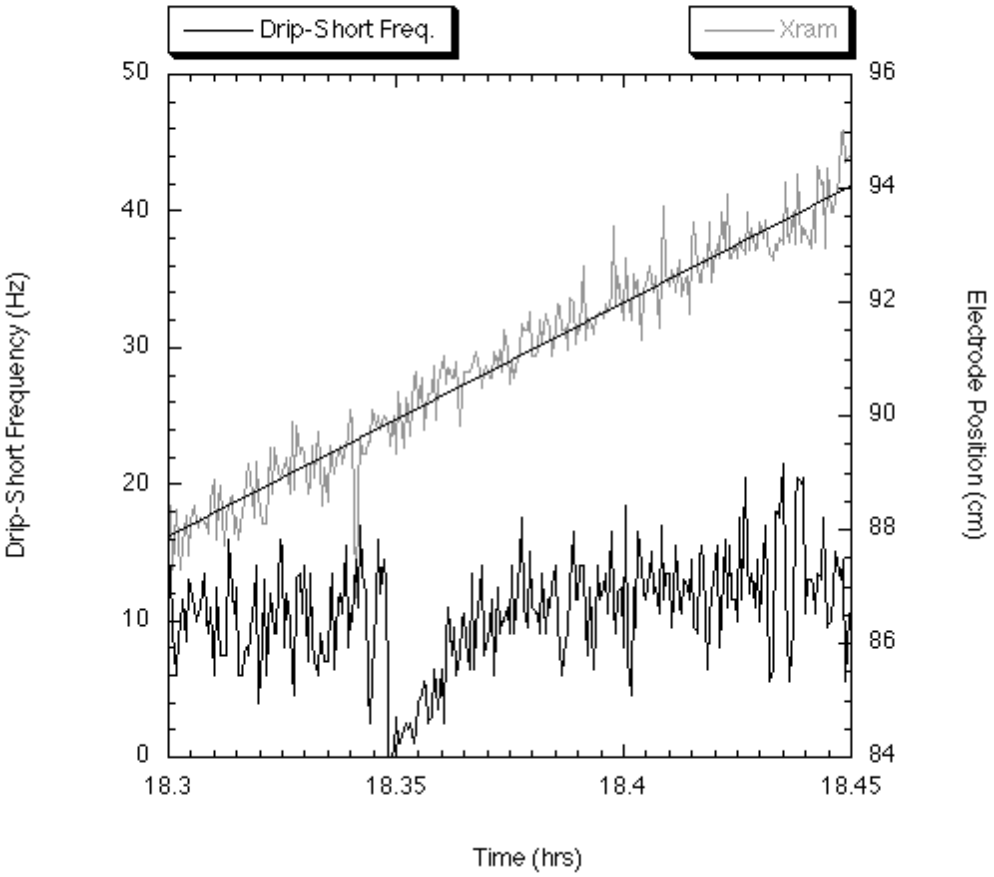

Figure 6. Plot of drip-short frequency and electrode position during the weld disturbance The straight line is the result of a linear regression analysis of the position data in this region.

Accurate estimation of melt rate from Eq. 5 requires that the electrode gap be held constant throughout the test period. It is clear from the drip-short data that, even though gap control could be further improved, the gap was not changing greatly during the test so that ram velocity is, indeed, a good indicator of average melt rate. In connection with this, note from Figure 5 that no significant change in drip-short frequency is observed at the moment of the commanded melt rate step.

Dynamic, closed loop melt rate control without a load cell represents a significant step forward in VAR process control. It relies on the low order melting model incorporated into the VAR estimator.[3] The estimator outputs values for the thermal boundary layer, electrode gap and process efficiency that are consistent with the process model given the estimator inputs. Thus, the estimated variables are constrained to lie within ranges permitted by physics. In this sense, the estimator behaves like a filter. For example, the "measured" electrode gap value may change by 0.01 m during a single time step. However, given the process inputs, measurements, and associated noise strengths, the filter "knows" that, according to the model, such a large change in gap over this time period is physically impossible, and the estimated gap is adjusted by a much smaller amount. This illustrates the power of Kalman filtering.[6]

SUMMARY AND CONCLUSIONS

A feedback melt rate controller was implemented on a small VAR furnace at Los Alamos National Laboratory that is not equipped with a functioning load cell transducer. A 0.127 m diameter 304 SS electrode was melted into 0.165 diameter ingot at a commanded melt rate of 27 g/s. The actual average melt rate, acquired from analyzing electrode position data, was 26.0±0.5 g/s. A melt rate step to 32 g/s was commanded near the end of the melt. The actual average melt rate was computed to be 31.4±1.8 g/s. Furthermore, the controller did a reasonable job of controlling melt rate through a melting disturbance associated with a weld in the electrode. The data demonstrate that feedback melt rate control without a load cell was achieved.

ACKNOWLEDGEMENT

Portions of this work carried out at Sandia National Laboratories were supported by the United States Department of Energy under Contract DE-AC04-94AL85000. Sandia National Laboratories is a multiprogram laboratory operated by Sandia Corporation, a Lockheed Martin Company, for the United States Department of Energy. Work carried out at Los Alamos National Laboratory was supported by the United States Department of Energy under Contract W-7405-ENG-36. Los Alamos National Laboratory is operated by The University of California for the United States Department of Energy. Additional support was provided by the Specialty Metals Processing Consortium.

REFERENCES

1. Bertram, L.A. and Zanner, F.J. "Electrode Tip Melting Simulation during Vacuum Arc Remelting of Inconel 718", in *Modeling and Control of Casting and Welding Processes*, S. Kou and R Mehrabian, eds., TMS, Warrendale, PA., 1986, p. 95.

2. Lee A. Bertram, John A. Brooks, David G. Evans, Ashish D. Patel, James A. Van Den Avyle, and Dwight D. Wegman, "Transient Melt Rate Effects On Solidification During VAR Of 20 Inch Alloy 718," *Proceedings of The 1999 International Symposium On Liquid Metal Processing And Casting*, Alec Mitchell, Lisa Ridgway, and Michael Baldwin, editors, Vacuum Metallurgy Division of the American Vacuum Society, 1999, pp. 156-67.

3. Joseph J. Beaman and Rodney L. Williamson, "A Nonlinear, Reduced Order Model for Dynamic Melt Rate Control," *Proceedings of The 2001 International Symposium On Liquid Metal Processing And Casting*, Alec Mitchell, editor, Vacuum Metallurgy Division of the American Vacuum Society, 2001.

4. L.A. Bertram, R.L. Williamson, D.K. Melgaard, J.J. Beaman, and D.G. Evans, "Dynamic Control of Remelting Processes," U. S. Patent No. 6,115,404, Sept. 5, 2000.

5. Rodney L. Williamson, Frank J. Zanner and S. M. Grose, "Arc Voltage Distribution Properties as a Function of Melting Current, Electrode Gap, and CO Pressure during Vacuum Arc Remelting," *Metall. And Mat. Trans. B*, 28B, 1997, pp. 841-53.

6. For examples of Kalman filtering applied solely to the electrode gap control problem, see C. L. Hysinger, J. J. Beaman, R. L. Williamson and D. K. Melgaard, "Multiple Input Electrode Gap Control during Vacuum Arc Remelting", *Proceedings of the 1999 International Symposium On Liquid Metal Processing and Casting*, Alec Mitchell, Lisa Ridgeway, and Michael Baldwin, editors, Vacuum Metallurgy Division of American Vacuum Society, 1999,

pp. 145-55; also R. L. Williamson, J. J. Beaman and D.K. Melgaard, “Optimal Estimation Of Electrode Gap During Vacuum Arc Remelting,” in *Proceedings of the 2001 EPD Congress*, TMS, P.R. Taylor, ed., New Orleans, LA, Feb. 2001, pp. 615-28.